Received: 2 October 2023 | Revised: 7 February 2024 | Accepted: 13 February 2024

DOI: 10.1002/nme.7482

RESEARCH ARTICLE

WILEY

Extension of the *a posteriori* finite element method (APFEM) to geometrical alterations and application to stochastic homogenisation

Yanis Ammouche | **Antoine Jérusalem**

Department of Engineering Science, University of Oxford, Oxford, UK

Correspondence
Antoine Jérusalem, Department of Engineering Science, University of Oxford, Parks Road, Oxford, OX1 3PJ, UK.
Email: antoine.jerusalem@eng.ox.ac.uk

Funding information
Engineering and Physical Sciences Research Council, Grant/Award Number: EP/S005072/1

Abstract

We recently proposed an efficient method facilitating the parametric study of a finite element mechanical simulation as a postprocessing step, that is, without the need to run multiple simulations: the a posteriori finite element method (APFEM). APFEM only requires the knowledge of the vertices of the parameter space and is able to predict accurately how the degrees of freedom of a simulation, i.e., nodal displacements, and other outputs of interests, for example, element stress tensors, evolve when simulation parameters vary within their predefined ranges. In our previous work, these parameters were restricted to material properties and loading conditions. Here, we extend the APFEM to additionally account for changes in the original geometry. This is achieved by defining an intermediary reference frame whose mapping is defined stochastically in the weak form. Subsequent deformation is then reached by correcting for this stochastic variation in the reference frame through multiplicative decomposition of the deformation gradient tensor. The resulting framework is shown here to provide accurate mechanical predictions for relevant applications of increasing complexity: (i) quantifying the stress concentration factor of a plate under uniaxial loading with one and two elliptical holes of varying eccentricities, and (ii) performing the stochastic homogenisation of a composite plate with uncertain mechanical properties and geometry inclusion. This extension of APFEM completes our original approach to account parametrically for geometrical alterations, in addition to boundary conditions and material properties. The advantages of this approach in our original work in terms of stochastic prediction, uncertainty quantification, structural and material optimisation and Bayesian inferences are all naturally conserved.

KEYWORDS

APFEM, geometrical uncertainties, nonlinear stochasticity, stochastic homogenisation

1 | INTRODUCTION

Manufacturing processes inevitably introduce geometrical imperfections to structural components. For example, curing, one of the most dominant and mature processes to assemble composites in the aeronautical industry[1] introduces uncertainties in both material properties and structural shape, arising, for example, for epoxy-based composites, from chemical and thermal shrinkage.[2] Despite important numerical and experimental efforts to reduce process-induced randomness,[3,4] geometrical deviations remain. Similarly, the recent promises of additive manufacturing (AM) to overcome many of these traditional manufacturing challenges by delivering materials with superior properties through complex topologies[5] have been dented by deviations from the targeted geometries. Those arise from the complex melting-cooling material processes inherent to AM, in turn strongly influencing the overall mechanical response.[6] Notwithstanding the need to refine these experimental methods for better predictability, it is of relevance to establish methods to quantify how topological alterations alter the overall mechanical integrity of manufactured components.

One straightforward approach is to rely on a Monte Carlo (MC) algorithm, whereby the different geometrical alterations are sampled and a deterministic simulation is run for each one of them. For example, Zhang et al.[7] successfully modelled and quantified the impact of brain interface topology perturbations to simulate the electrical field in brain tissues using MC. Although this method is flexible and scales well with higher dimension, it requires remeshing and converges slowly.[8] As a result, numerous expensive deterministic simulations are often needed to ensure adequate accuracy. To this end, more efficient and sophisticated frameworks have been proposed, though MC methods are still often relied upon to verify solutions obtained with those. Wang et al.[9] used a Kriging surrogate model based on polynomial chaos expansion (PCE)[10] to efficiently capture the random response of a turbine blade with geometrical variations. Sakata et al.[11] considered a heterogeneous material with random position of a parametrised inclusion. Using the perturbation method, the authors obtained linearised solutions of the homogenised quantities. However, this method is restricted to the propagation of small uncertainties. Pivovarov and Steinmann[12] developed an homogenisation strategy for composites with moderate to high amplitude of geometrical uncertainties in the microstructure. The material properties were described with a stochastic level-set function defining whether a given point belongs to the matrix or the inclusion. Though accurate, this method is dependent on a user-defined smoothness coefficient. The fictitious domain method, see, for example, the work of Canuto and Kozubek,[13] solves PDEs on a single, fictitious domain encompassing all possible outcomes of the physical domain. The PDEs are reformulated as a saddle point problem where auxiliary variables (Lagrange multipliers) are introduced. Nouy et al.[14] built on this approach to propose the extended stochastic finite element method (X-SFEM) where the random geometry is modelled using random level-set functions. Doing so, an accurate stochastic solution was obtained using Galerkin approximation for a plate of random geometry under tensile loading. While this method avoids remeshing, complex partitioning of the stochastic domain is still required.

Instead of using fictitious domains, a method that often requires computation of additional variables, Acharjee and Zabaras[15] used intrusive methods[16] for geometrical uncertainty propagation where a simple hole was introduced using a uniform random variable. An excellent match with ground truth results, obtained with MC, was observed, but few theoretical details about the framework were published. Mohan et al.[17] mapped a random domain onto a deterministic reference domain for the simulation of heat transfer in a turbine with uncertain geometry of the cooling core. While the stochastic response of the simulation was captured with satisfying accuracy, this method cannot tackle problems with both random geometry and material property uncertainties. Zheng et al.[18] developed a framework to solve stochastic PDEs on random domains using a mapping algorithm, similarly to the work of Mohan et al.[17] The stochastic solution was obtained using a non-intrusive method, requiring numerous evaluations of the stiffness matrix and the force vectors. This approach can be seamlessly integrated to any commercial software while keeping a reasonable number of terms in the expansion of the random solution when increasing the input parameter space dimension. Nevertheless, the iterative procedure to compute the deterministic coefficient and the stochastic germs of the solution is cumbersome and sampling-dependent.

Here, we introduce an enhanced version of the previously proposed a posteriori finite element method (APFEM)—a stochastic method where parameter uncertainties are embedded in the weak form—by efficiently handling geometrical imperfections through a two-step calculation process. APFEM takes as input the vertices of the parameter space of interest and predicts the variation of the degrees of freedom of a simulation, i.e., nodal displacements, as well as other outputs of interests, for example, element stress tensors, as the simulation parameters vary within these ranges and as a postprocessing step, that is: the simulation is only run once. In its original version, these parameters were restricted to material properties and loading conditions. This extension of APFEM leverages the strengths of the previous method, i.e., the ability to express nodal coordinates and elemental stress as polynomials of the unknown parameters in nonlinear

mechanical contexts, while now allowing for topological uncertainty. To this end, the uncertainty is (i) formulated as an analytical stochastic displacement of the model boundary, leading to (ii) an intermediate state corresponding to the resulting stochastic deformation of the mesh, then taken as a (iii) a stress-free configuration from which the mechanical deformation corresponding the the physics of the problem is then predicted. The new approach is first presented in detail and shown to be both straightforward and flexible, as it solely requires the analytical expression of the geometrical alteration. Three applications are then presented to illustrate the flexibility of the method and its relevance to stochastic homogenisation: first, a plate with a hole of variable eccentricity is loaded under a deterministic load; a plate with two holes under similar conditions is then proposed in the context of multiple holes simulation; a stochastic homogenisation of a composite material with varying material properties and inclusion shapes is finally presented.

2 | GENERAL FRAMEWORK

In the following, we first briefly recall the theoretical framework of APFEM, and follow with a description of its formulation to random geometries.

2.1 | APFEM

APFEM was first proposed by the authors as a specialisation of the Galerkin stochastic finite element method (GSFEM). In the following, we very briefly review the method, while referring the reader to the work of Ammouche and Jérusalem[19,20] for more details. The GSFEM, originally pioneered by Ghanem and Spanos,[16] expands the stochastic solution of a given boundary value problem solved with the finite element method by using PCE whose deterministic coefficients are obtained in an intrusive manner, i.e., by establishing an algebra for stochastic operations and redefining the constitutive models accordingly. The finite element displacement function $\boldsymbol{u}$ is thus written as follows:

$$\boldsymbol{u}(\boldsymbol{x},\theta) = \sum_a N_a(\boldsymbol{x})\boldsymbol{u}^a = \sum_a N_a(\boldsymbol{x}) \sum_\epsilon \Psi_\epsilon(\theta)\boldsymbol{u}^{a\epsilon}, \tag{1}$$

where N_a are the usual finite element shape functions, Ψ_ϵ the shape functions associated to the stochastic space and $\boldsymbol{u}^{a\epsilon}$ the stochastic component ϵ^* of the displacement of node a. The dependence on θ denotes a function on the probability space. As such, two Galerkin projections are performed to determine both spatial and stochastic components of the displacement. Finally, the Askey-Wiener scheme[21] is used to choose the appropriate PCE (the Ψ_ϵ) for optimal convergence[22] depending on the input parameter distributions. GSFEM can thus be used to determine the probability distribution of the simulation's outputs when the inputs' distribution is known. APFEM focuses instead on establishing a framework where ranges of input parameters are embedded in the solver so as to allow for a posteriori exploration of the effect of input parameter changes on the finite element solution. This is achieved by adopting a uniform distribution which ensures an equally distributed weight of the finite element error across the range of interest, then only defined through its bounds. Following Xiu and Karniadakis,[21] the multivariate polynomials Ψ_ϵ in Equation (1) are taken to be Legendre polynomials, thus ensuring exponential convergence.[22]

Briefly, APFEM considers a multivariate random variable $\boldsymbol{\theta} = [\theta_1, \dots, \theta_N]$, where $\theta_i: \Theta \to E$, $\forall i \in [1, N]$, with Θ the sample space of a probability triple $(\Theta, \mathrm{A}, \mathbb{P})$ with a σ-algebra A, probability measure $\mathbb{P}$, for a support E. The cumulative distribution function (CDF) $\mathbb{P}_\theta$ of $\boldsymbol{\theta}$ is defined as follows:

$$\mathbb{P}_{\boldsymbol{\theta}}(\boldsymbol{w}) = \mathbb{P}(\theta_1 \le w_1, \dots, \theta_N \le w_N), \tag{2}$$

where $\boldsymbol{w} = [w_1, \dots, w_N]$. The weak form of the balance of linear momentum can be formulated as: for all arbitrary admissible virtual stochastic displacement $\boldsymbol{\eta}$, with $\boldsymbol{\eta}(\boldsymbol{X},\theta) = \boldsymbol{0}$ almost surely for all $\boldsymbol{X} \in \partial\Omega_0^d$, where $\partial\Omega_0^d$ represents the domain boundary where Dirichlet boundary conditions (BCs) are applied,

$$\begin{aligned}\int_{E^N}\int_{\partial\Omega_n} \overline{P}\boldsymbol{n}\cdot\boldsymbol{\eta}\,\mathrm{d}S\mathrm{d}\mathbb{P}_\theta(\boldsymbol{w}) + \int_{E^N}\int_{\Omega_0} \rho_0\boldsymbol{b}\cdot\boldsymbol{\eta}\,\mathrm{d}V_0\mathrm{d}\mathbb{P}_\theta(\boldsymbol{w}) \\ = \int_{E^N}\int_{\Omega_0} \boldsymbol{P} : \mathrm{Grad}\,\boldsymbol{\eta}\,\mathrm{d}V_0\mathrm{d}\mathbb{P}_\theta(\boldsymbol{w}) + \int_{E^N}\int_{\Omega_0} \rho_0\ddot{\boldsymbol{u}}\cdot\boldsymbol{\eta}\,\mathrm{d}V_0\mathrm{d}\mathbb{P}_\theta(\boldsymbol{w}),\end{aligned} \tag{3}$$

where $\boldsymbol{b}$ represents the body forces, ρ_0 the mass density, $\overline{P}$ the applied pressure as Neumann BCs on $\partial\Omega^n$ where $\boldsymbol{n}$ is the normal in the deformed reference frame, and $\boldsymbol{P}$ the first Piola–Kirchhoff stress tensor; all a priori stochastic in nature. More details about alternative choice of interpolants, numerical implementation and potential applications of the APFEM can be found in the work of Ammouche and Jérusalem.[19,20]

2.2 | APFEM extension to random domains

This section details the proposed strategy to solve stochastic PDEs on random domains using APFEM. Here and subsequently, we assume that is possible to characterise all possible geometrical configurations using an analytical function M. In the context of APFEM, only uniform random distribution are contributing to the randomness of the function M (note that a similar extension straightforwardly applies to GSFEM). The knowledge of M allows the creation of a mapping between the initial reference domain Ω_0 and all possible realisations of the stochastic domain Ω_0^s using a given number of parameters, all comprised between -1 and 1 without loss of generality. In the first step of the framework, the mapping is obtained by solving the equilibrium Equation (3) with Dirichlet BCs defined by M. This step essentially displaces stochastically all the nodes inside the mesh as a response to the stochastic displacement M on its boundary. While the solution of this first step depends on the constitutive model being used, we will demonstrate that the second step of the framework corrects for this and that this first step is in fact akin to a stochastic remeshing. As a second step, the boundary value problem involving loading conditions is solved to obtain the stochastic response as a function of the random geometry. This second step, however, corrects the deformation gradient tensor to make it independent of the stochastic deformation gradient tensor of the first step, see Figure 1. This is achieved through multiplicative decomposition of the deformation tensor $\boldsymbol{F}$ as:

$$\boldsymbol{F} = \boldsymbol{F}_{\text{Mech}} \cdot \boldsymbol{F}_{\text{Map}}, \tag{4}$$

where $\boldsymbol{F} = \boldsymbol{I} + \nabla \boldsymbol{u}$, $\boldsymbol{F}_{\text{Map}}$ maps Ω_0 onto Ω_0^s and $\boldsymbol{F}_{\text{Mech}}$ is the "mechanical" component of $\boldsymbol{F}$ being used in the second step of the proposed framework. Indeed, as the intermediate configuration is stress-free, the Piola–Kirchhoff stress tensor $\boldsymbol{P}$ is only dependent on $\boldsymbol{F}_{\text{Mech}} = \boldsymbol{F} \cdot \boldsymbol{F}_{\text{Map}}^{-1}$. Equation (3) is then simply reformulated with the intermediary reference frame

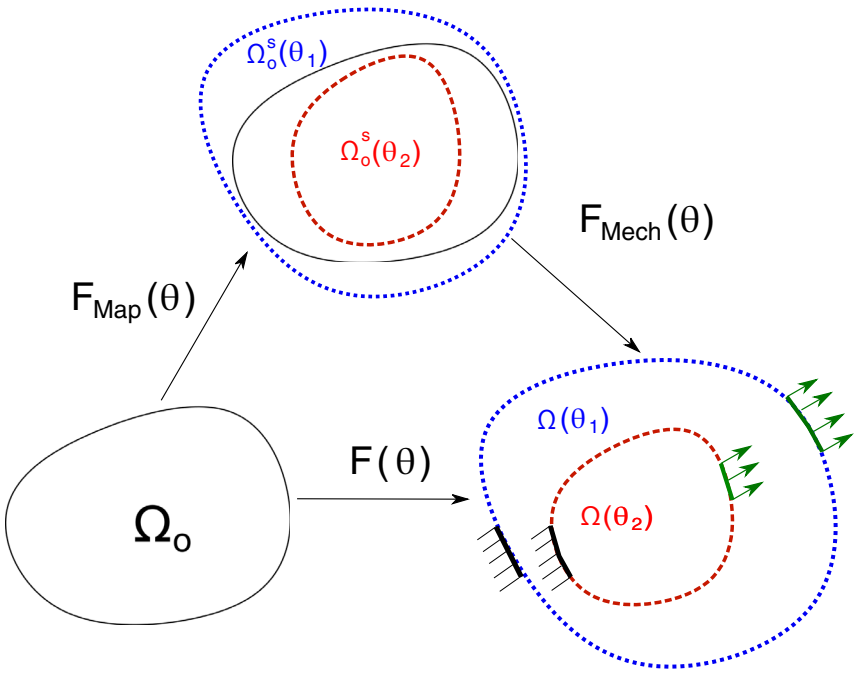

FIGURE 1 Scheme of the APFEM extension to random domains. In blue and red are shown two possible realisations of the random geometry.

as the stress-free configuration as:

$$\int_{\boldsymbol{E}^N}\int_{\partial\Omega_n}\overline{P}\boldsymbol{n}\cdot\boldsymbol{\eta}_{\text{Mech}}\,\mathrm{d}S\mathrm{d}\mathbb{P}_\theta(\boldsymbol{w})+\int_{\boldsymbol{E}^N}\int_{\Omega_0}\rho_0\boldsymbol{b}\cdot\boldsymbol{\eta}_{\text{Mech}}\,\mathrm{d}V_0^s\mathrm{d}\mathbb{P}_\theta(\boldsymbol{w})$$
$$=\int_{\boldsymbol{E}^N}\int_{\Omega_0^s}\boldsymbol{P}(\boldsymbol{F}_{\text{Mech}}):\text{Grad}\,\boldsymbol{\eta}_{\text{Mech}}\cdot\boldsymbol{F}_{\text{Map}}^{-1}\,\mathrm{d}V_0^s\mathrm{d}\mathbb{P}_\theta(\boldsymbol{w})+\int_{\boldsymbol{E}^N}\int_{\Omega_0^s}\rho_0\ddot{\boldsymbol{u}}_{\text{Mech}}\cdot\boldsymbol{\eta}_{\text{Mech}}\,\mathrm{d}V_0^s\mathrm{d}\mathbb{P}_\theta(\boldsymbol{w}), \tag{5}$$

where the subscript $_{\text{Mech}}$ refers to the mapping from Ω_0^s. We note that ρ_0 and $\boldsymbol{b}$ are solely defined in that mapping, and as such the subscript is ignored for these. Similarly, as this equation is true for all admissible virtual displacements $\boldsymbol{\eta}_{\text{Mech}}$, the subscript is dropped subsequently. As the stochastic component of the nodal displacement is time-invariant, $\ddot{\boldsymbol{u}}_{\text{Mech}}$ can be replaced by $\ddot{\boldsymbol{u}}$. Finally, the additional $\boldsymbol{F}_{\text{Map}}^{-1}$ in the first term of the right-hand side arises from the fact that the Grad operator is defined in the original reference frame Ω_0. Accounting for this, and changing the integral to the original reference frame to retain the Lagrangian implementation of the framework leads to:

$$\int_{\boldsymbol{E}^N}\int_{\partial\Omega_0^n}J\boldsymbol{F}^{-T}\overline{P}\boldsymbol{N}\cdot\boldsymbol{\eta}\,\mathrm{d}S_0\mathrm{d}\mathbb{P}_\theta(\boldsymbol{w})+\int_{\boldsymbol{E}^N}\int_{\Omega_0}\rho_0J_{\text{Map}}\boldsymbol{b}\cdot\boldsymbol{\eta}\,\mathrm{d}V_0\mathrm{d}\mathbb{P}_\theta(\boldsymbol{w})$$
$$=\int_{\boldsymbol{E}^N}\int_{\Omega_0}J_{\text{Map}}\boldsymbol{P}(\boldsymbol{F}_{\text{Mech}})\cdot\boldsymbol{F}_{\text{Map}}^{-T}:\text{Grad}\,\boldsymbol{\eta}\,\mathrm{d}V_0\mathrm{d}\mathbb{P}_\theta(\boldsymbol{w})+\int_{\boldsymbol{E}^N}\int_{\Omega_0}\rho_0J_{\text{Map}}\ddot{\boldsymbol{u}}\cdot\boldsymbol{\eta}\,\mathrm{d}V_0\mathrm{d}\mathbb{P}_\theta(\boldsymbol{w}), \tag{6}$$

for all admissible virtual displacement $\boldsymbol{\eta}$, and where $J_{\text{Map}}=\det\boldsymbol{F}_{\text{Map}}$, $J=\det\boldsymbol{F}$ and $\boldsymbol{N}$ is the normal to the Neumann boundary in the original reference frame.

In practice, the discretisation of Equation (6) and implementation in a APFEM code can be done straightforwardly by mapping the different quantities against the terms in Equation (3).

3 | APPLICATIONS

3.1 | Plate under tension with a single hole

In this section, we revisit the case of a plate with a hole under tension. This example is often used as an illustration of the potentially catastrophic effect of a hole (or more generally, defect) in a structure, by considering the so called stress concentration factor (SCF)[23,24] defined as the ratio of the local increased stress (typically around the hole) to the stress applied to the overall structure. While an analytical solution exists when the hole is elliptic, small with respect to the structure, and the material is linear elastic,[25] there is no straightforward solution when other shapes or additional BCs are considered. To estimate the variation of SCF with respect to geometrical parameters of the hole, Tong et al.[26] performed repeated finite element simulations to obtain a regression of the SCF as a function of key hole parameters in concrete-filled square hollow section joints. While machine learning methods have also been used to establish similar relations,[27] they still rely on training data and potentially many simulations. Here, we leverage the proposed framework to obtain the stress field and SCF for a range of geometrical configurations for a 2D plane stress holed plate clamped on its left side and submitted to a deterministic uniform loading on its right side, see Figure 2. The eccentricity of the hole is assumed to be random, and controlled by fixing one of the two axes of the ellipse (b) and varying the other axis (a), see Figure 2. Note that only half of the plate is considered by symmetry.

The first step of the framework consists in establishing a relationship between the original reference frame and the intermediary stochastic frame. This is done by applying the following stochastic Dirichlet BCs on the inner surface of the elliptic hole with a stochastic axis $a(\theta)$:

$$\begin{aligned}\text{BC}_x&=\frac{ab\cos(\varphi)}{\sqrt{b^2\cos^2(\varphi)+a^2\sin^2(\varphi)}}-b\cos(\varphi),\\ \text{BC}_y&=\frac{ab\sin(\varphi)}{\sqrt{b^2\cos^2(\varphi)+a^2\sin^2(\varphi)}}-b\sin(\varphi),\end{aligned} \tag{7}$$

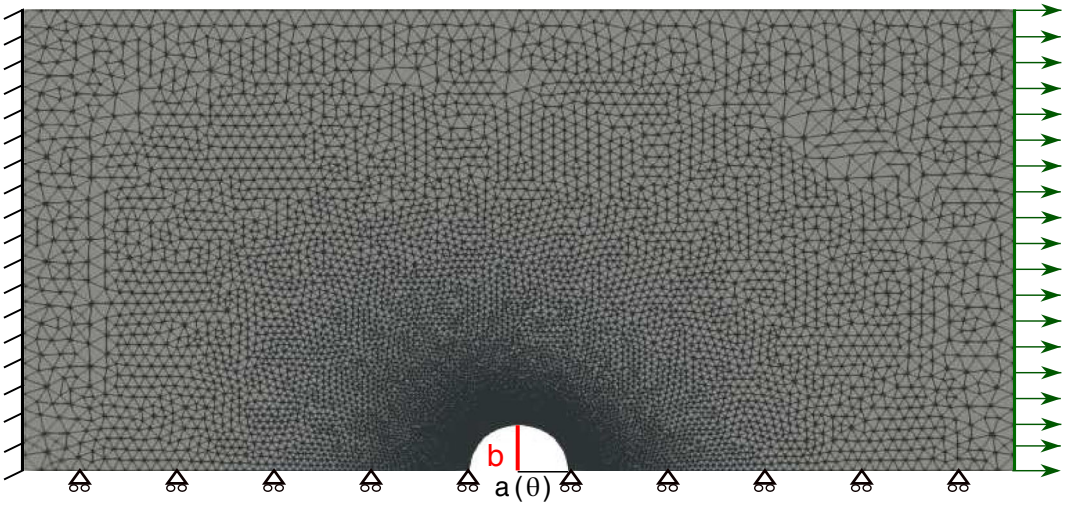

FIGURE 2 Plate with a hole of random dimensions, clamped on the left-hand side, and submitted to a deterministic pressure σ_0 on the right-hand side.

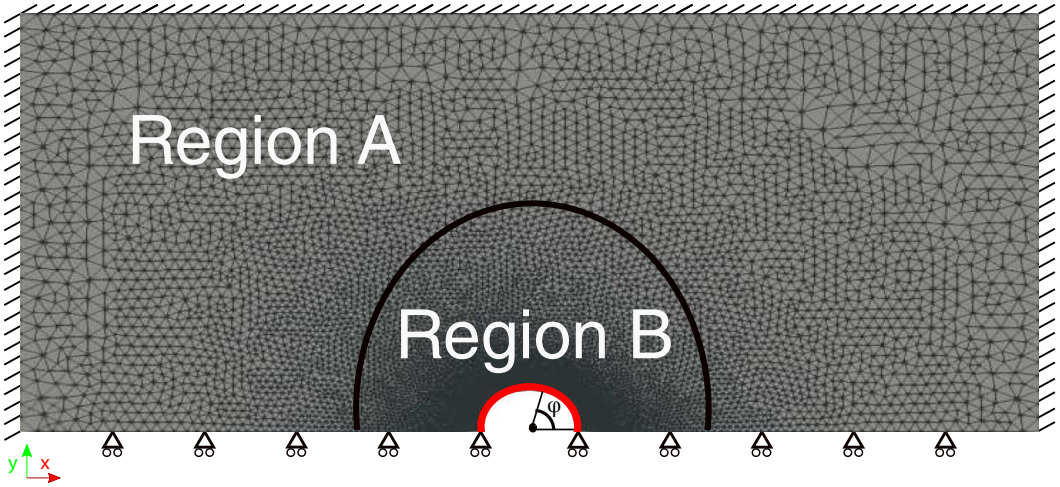

FIGURE 3 Stochastic loading of the random domain (first step), and proposed domain decomposition (A and B); in red: stochastic BCs, see Equation (7).

where φ is the angle between the position vector and the x-axis, b is the vertical (long) axis (fixed and deterministic) and $a(\theta) = \frac{b}{5}(4+\theta)$ is the horizontal axis of the ellipse, and θ varies between -1 and 1. The left, right and top boundaries are fully clamped, while the bottom boundary is constrained in y, see Figure 3.

The first step of the proposed framework solves for $\boldsymbol{F}_{\text{Map}}$ to be used in subsequent loading. So as to be compatible with APFEM's formulation, the Dirichlet BCs of Equation (7) need to be expressed as a PCE, for a flat random distribution of θ. Note that the use of nonlinear operators requires the use of a specific algebra already proposed by Debusschere et al.[28] and Ammouche and Jérusalem.[19]

By design, the random reference configuration is dependent on the constitutive law chosen during the first step as it involves a mesh deformation. This should a priori not influence the second (physical) step as the deformation gradient tensor is corrected to ensure a stress-free configuration in the random reference configuration. In the following, we assess this observation, by purposefully decomposing the plate into two regions A and B of different material properties, see Figure 3. We then study four cases with different Young's moduli in regions A and B using a Saint-Venant Kirchhoff constitutive model. Values used for these cases can be found in Table 1. The second loading step is, however, done with the same material properties for both regions, see Table 2. The mesh features are also provided in Table 2. As discussed above,

TABLE 1 Material parameters for the four different cases during the first step.

	Region A	Region B
Case 1	$E = 10^6$ Pa, $\nu = 0.3$	$E = 10^6$ Pa, $\nu = 0.3$
Case 2	$E = 10^7$ Pa, $\nu = 0.3$	$E = 10^7$ Pa, $\nu = 0.3$
Case 3	$E = 10^6$ Pa, $\nu = 0.3$	$E = 10^7$ Pa, $\nu = 0.3$
Case 4	$E = 10^7$ Pa, $\nu = 0.3$	$E = 10^6$ Pa, $\nu = 0.3$

TABLE 2 Finite element discretisation and geometrical features of the plate.

Parameters	Value
Geometrical features	Length = 10 m, width = 5 m
Number of nodes	32,669
Type of elements	Quadratic triangle (plane stress)
Number of elements	16,152
b	0.5 m
Range of a	0.3 to 0.5 m
PCE order	4
σ_0	10,000 Pa
Young's modulus and Poisson's ratio	10^7 Pa, 0.3

the intermediary configuration should be stress-free, meaning that independently of the material properties in Regions A and B, the final results of the simulation ought to be the same. The four cases proposed here aim at verifying this. All four simulations are then conducted and the predicted SCFs for all four cases are compared against the analytical solution:

$$\text{SCF} = \frac{Max(\sigma_{xx})}{\sigma_0} = 1 + 2\frac{b}{a}. \tag{8}$$

The displacements, strain and stress fields are obtained using a fourth-order PCE.

Figure 4A compares the SCF obtained with the proposed framework and the analytical solution given by Equation (8) (the plotted solutions for the APFEM was obtained by taking varying the parameter θ from -1 to 1). A good match between the APFEM for all four cases and the baseline solution is observed. Discrepancies originate from the approximation of the BCs in Equation (7) arising from the nonlinear PCE operations.[28] Indeed, as the terms in Equation (7) involve negative power of random variables, higher-order PCEs would be required for better accuracy, at the expense of computational cost. We can note that the results are weakly dependent on the first step, akin to a "remeshing" strategy (the change of stiffness between regions do modify the stochastic position of the nodes after the first step) leading to a mesh difference in the stress-free intermediary reference frame. The relative error between APFEM in Case 1 and any other cases remains smaller than half of a percent, see Figure 4B. Subsequently, we consider that the final result of this method does not depend on the constitutive law or material parameters used in the first step of the computation.

3.2 | Plate under tension with two holes

In this section we increase the complexity of the previous example by now considering two half holes of different shapes on both sides of the plate, leading to a topological variation parameterised by two parameters. Previous work has studied this particular problem in the context of "pitting corrosion",[29,30] where stochastic parameterisation of the topological problem is often needed. Indeed, Shi and Mahadevan[31] proposed a probabilistic method, using an analytical first-order reliability method and MC simulations, to obtain the CDF of the corrosion fatigue life from pit nucleation to fracture. Other studies have focused on the effect of pitting corrosion on the SCF for different positions and aspect ratio of pits. Cerit[32] predicted

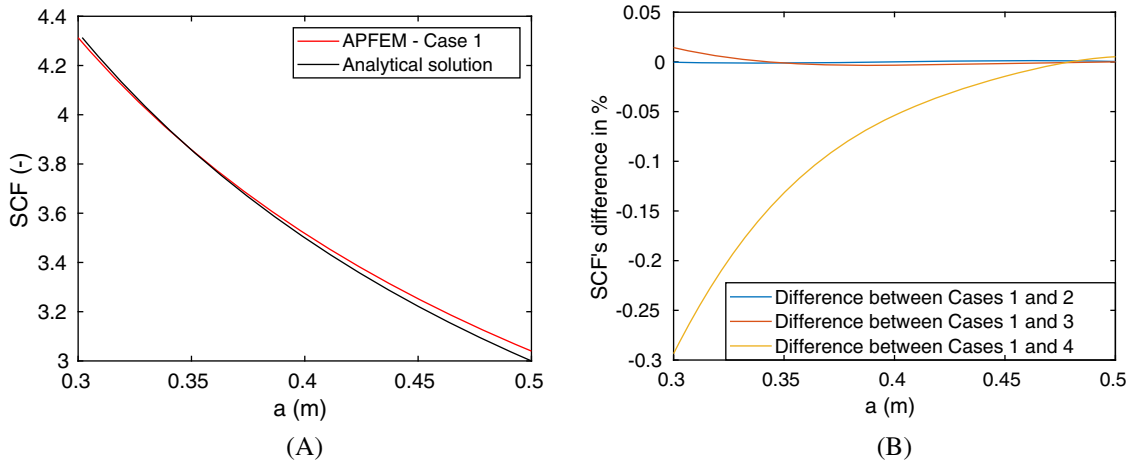

FIGURE 4 Evaluation of (A) APFEM's accuracy to capture geometrical uncertainties' effect and (B) robustness of APFEM framework with respect to the remeshing step. (A) Comparison of the SCF between APFEM and analytical solution. (B) Variation in predicted SCF for all four cases.

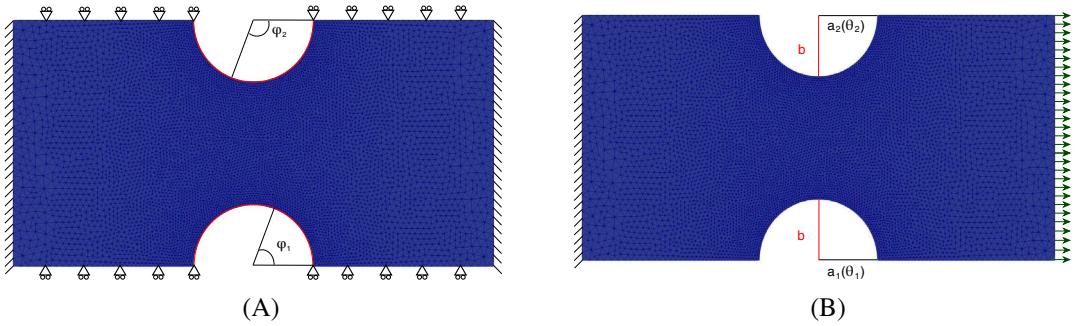

FIGURE 5 Scheme of the two-step computation for a plate with two random holes. (A) First step of the computation. The vertical edges are clamped while stochastic Dirichlet BCs are applied at the circular holes, see Equation (9). (B) Second step of the computation. A nominal stress σ_0 is applied on the right side of the plate and no displacement on the left.

the SCF of a spherical pressure vessel using multiple finite element simulations for various pit depths and diameters. Zuñiga Tello et al.[33] carried out a computational study with a double-pit model to quantify the influence of pit proximity, depths and component thickness on the SCF for aeronautical aluminium alloy AISI 7075-T under bi-axial loading. Li et al.[34] also performed parametric studies of pit-geometry on the SCF for cable steel wire. Most of these studies made use of MC. Here, we revisit the example of Section 3.1 by additionally studying the effect of an additional (independent) hole, under the same BCs, except for the top surface being constrained vertically, see Figure 5A.

We follow the same methodology as in the previous section: the first step imposes Dirichlet stochastic BCs to map the reference deterministic configuration, a plate with two circular holes, to a plate with two elliptic holes of random small axes, see Figure 5A, as follows:

$$\begin{aligned} \mathrm{BC}_x &= \frac{a_i b \cos(\varphi_i)}{\sqrt{b^2\cos^2(\varphi_i) + a_i^2 \sin^2(\varphi_i)}} - b\cos(\varphi_i), \\ \mathrm{BC}_y &= \chi(i)\frac{a_i b \sin(\varphi_i)}{\sqrt{b^2\cos^2(\varphi_i) + a_i^2 \sin^2(\varphi_i)}} - b\sin(\varphi_i), \end{aligned} \tag{9}$$

where $\chi(i) = 1$ if $i = 1$ (bottom hole) and -1 if $i = 2$ (top hole). In the second step, the plate is clamped on its left side and submitted to a uniform loading of intensity σ_0 on the right-hand side. The same constitutive law and parameters

TABLE 3 Finite element discretisation and geometrical features of the plate.

Parameters	Value
Geometrical features	Length = 4 m, width = 2 m
Number of nodes	26,855
Type of elements	Quadratic triangle (plane stress)
Number of elements	13,244
b	0.5 m
Range of a_1	0.3 to 0.5 m
Range of a_2	0.3 to 0.5 m
PCE order	4
σ_0	10,000 Pa

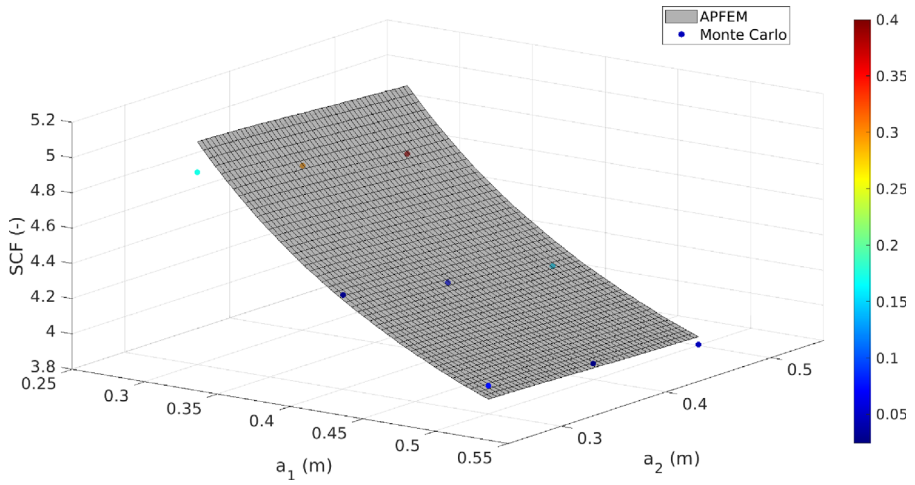

FIGURE 6 SCF surface response for hole 1 versus a_1 and a_2 using APFEM and MC; the colour legend corresponds to the absolute error between APFEM and baseline MC simulations.

for both steps are used here, and correspond to the ones chosen in the second step of the previous section, see Table 2. The finite element discretisation, geometrical features and stochastic parameters are given in Table 3. Figure 6 shows the APFEM-predicted SCF for different combinations of a_1 and a_2 and the MC counterparts (used here as the baseline, as there is no straightforward analytical solution). The prediction of the SCF for hole 1 given by APFEM shows a good accuracy when compared to MC simulations. However, APFEM's precision decays when increasing the value of a_2, as the error can reach a maximum of 0.4 (which still remains below ~10% in relative error). The discrepancies is thought to arise from the projection of Equation (9) in the PCE space. Of note: the SCF is shown to be maximum when pits become narrower, that is, $a_1 = a_2 = 0.3$ m.

3.3 | Stochastic homogenisation

In this section, we illustrate the viability of the proposed framework for stochastic homogenisation in the context of composites. Composites are widely used in the industry for their superior strength/density ratio (specific strength). A vast body of literature has been concerned with the quantification of composites' response under structural uncertainties, see, for example, the recent work of Stefanou et al.[35] and Thapa and Missoum.[36] However, these often rely on non-intrusive methods, such as MC, and are thus subjected to the limitations discussed above. Here, we make use of APFEM to study a 2D composite with random material parameters and inclusion elliptical topology. Rosić et al.[37] have shown that intrusive methods fail to model accurately problems involving plasticity with typical rate-independent formulations. The issue arises from the need to determine whether plasticity occurs at a material point, a step that is often done by comparing

a stress quantity (typically the von Mises stress) against a criterion (typically the yield stress), an operation that is not uniquely defined in a stochastic framework. The approximation then adopted by the modeller (e.g., with a cutoff in the tail of a stress distribution to delimitate the position of the distribution with respect to a value) introduces a nonrecoverable deviation from the true solution, even when increasing the PCE order. Building on the study of Acharjee and Zabaras,[15] we use instead a visco-elastoplastic (thus rate dependent) formulation relying on the non-explicit formulation of the yield criterion through a power law, thus bypassing the shortcomings mentioned above, see Appendix A.

Here, we consider a heterogeneous material with a high inclusion-matrix stiffness ratio. Both inclusion topology and material properties are considered stochastic. The stochasticity of the former is done by imposing the same Dirichlet BCs as in the previous applications (see Equation (7)) onto the boundary between inclusion and matrix as the first step of the framework (the law and material parameters for the first step are the same as in the previous cases), see Figure 7A. The latter is done in the second step, where the Saint-Venant Kirchhoff visco-elastoplastic model is used to describe the mechanical behaviour of the inclusion and the matrix of the composite during the second step of the computation, see Appendix A for formulation. A deterministic uniaxial tensile loading (displacement loaded u_0 on the right, and clamped on the left) is applied, see Figure 7B. We assume the Young's moduli of each phase to be independent variables with an elliptic inclusion of random small axis value (also independent). The finite element discretisation, geometrical features and constitutive parameters are shown in Tables 4 and 5.

The APFEM simulation required 33.66 h on 40 AMD EPYC™7642 cores, that is, 1346 core h, while one deterministic simulation requires 134 s (so 1/900th of the time, that is, a Monte Carlo approach with 900 simulations would take the same amount of resources as one APFEM simulation, though without accounting for the remeshing), for comparison. Figure 8A,B show the isosurfaces of the homogenised Young's modulus and yield stress (as defined by the 0.2% offset criterion), respectively, of the composite with respect to the Young's moduli of the matrix and inclusion, and the small axis of the elliptical inclusion. The results obtained with APFEM show that the inclusion stiffness has a major influence on the overall composite stiffness. Unsurprisingly, the small axis in this particular case has little influence on the homogenised Young's modulus (as aligned with the loading direction in this case). The matrix and inclusions stiffnesses, however, have a clear influence on the overall stiffness. The study on the yield surface is also of interest as it demonstrates that a range of combinations of matrix and inclusion stiffness and inclusion geometry can be utilised for a target yield stress, see Figure 8B. Finally, Figure 9 shows the homogenised yield stress for a range of inclusion stiffness and shape for a matrix Young's modulus of 8 MPa. As can be seen on this figure, the approach straightforwardly allows to design an inclusion shape for a given stiffness when wanting to maximise the composite yield stress. Again, it must be emphasised that these analyses are all done as a postprocessing step, and no additional simulation is needed.

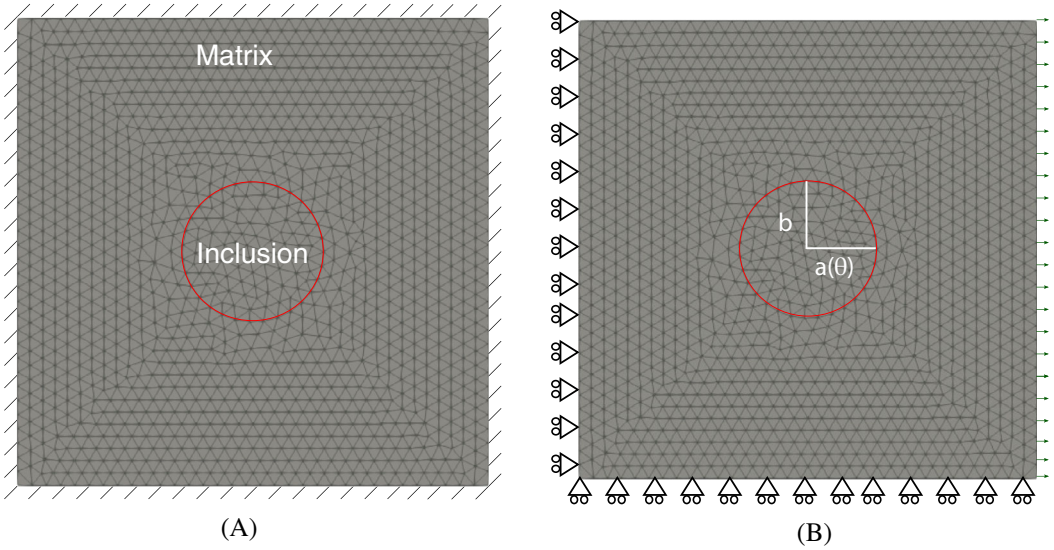

FIGURE 7 Scheme of the two-step framework for composite's homogenisation. (A) First step: Mapping between the initial and stochastic intermediary frames by clamping all sides while imposing stochastic Dirichlet BCs at the matrix-inclusion boundary (red circle). (B) Second step: Uniaxial deformation with stochastic material parameters by imposing a nominal displacement u_0 on the right side of the plate, no horizontal displacement on the left side and no vertical displacement on the bottom.

TABLE 4 Finite element discretisation and geometrical features of the composite.

Parameters	Value
Geometrical features	Length = 1 m, width = 1 m
Number of nodes	1306
Type of elements	Quadratic triangles (plane stress)
Number of elements	2478
b	0.15 m
Range of a	0.135 to 0.165 m
PCE order	3
u_0	0.20 m

TABLE 5 Constitutive model and parameters of the composite's phases, see also Appendix A.

	Inclusion	Matrix
Constitutive model	Saint-Venant Kirchhoff	Visco-elastoplastic
Range of Young's modulus	4.5×10^8 to 5.5×10^8 Pa	7.2×10^6 to 8.8×10^6 Pa
Poisson's ratio	$\nu = 0.4$	$\nu = 0.3$
Plasticity parameters		$\dot{\varepsilon_0} = 0.002\ \mathrm{s}^{-1}$, $s = 4.5 \times 10^5$ Pa, $n = 5$

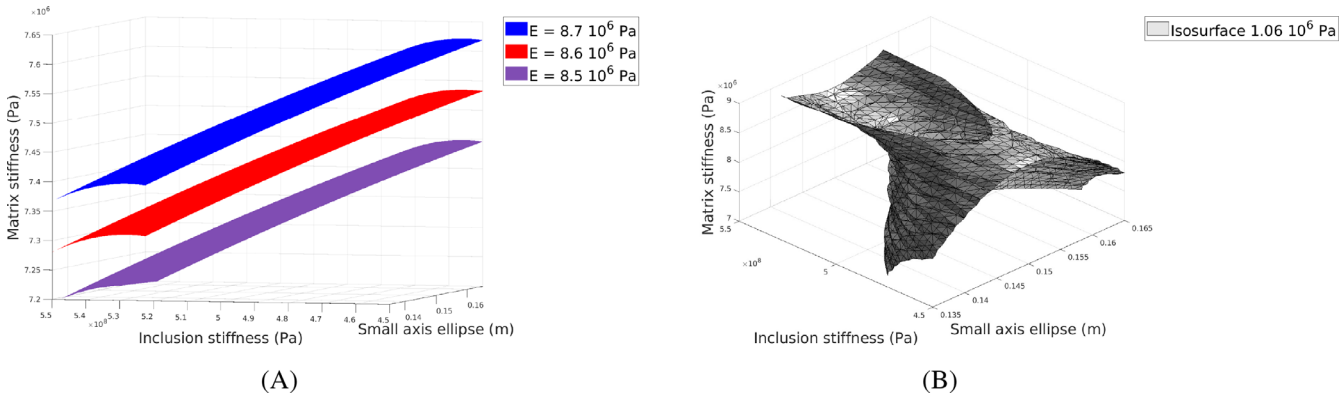

FIGURE 8 Isosurface of the homogenised Young's modulus and yield stress. (A) Isosurfaces of the homogenised Young's modulus. (B) Isosurface $\sigma_{\text{yield}} = 1.06 \times 10^6$ Pa.

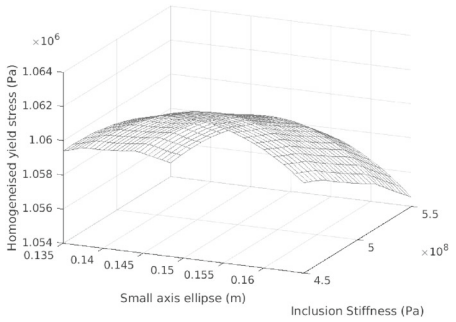

FIGURE 9 Homogenised yield stress versus inclusion shape and stiffness, for a matrix Young's modulus of 8 MPa.

4 | DISCUSSION

In this work, we broadened the scope of the previously proposed APFEM to incorporate the possibility of modelling structural components behaviour with limited topology knowledge. Similarly to the previously developed APFEM, solely the vertices of the parameter space are required. With these bounds' knowledge, APFEM allows for efficient and accurate predictions of mechanical outcomes at every point comprised between those bounds. However, assuming that the precise distribution of input parameters is available, a similar extension of GSFEM can be seamlessly obtained by considering the appropriate polynomial interpolants in Equation (1). The proposed framework does not rely on any remeshing algorithm or repeated deterministic simulations. Instead, a mapping from an initial deterministic configuration into a stochastic intermediary frame, accounting for all possible geometries, is obtained by solving equilibrium equations. Subsequently, the usual mechanical loading of the previous APFEM is applied on this stochastic, stress-free intermediate configuration, potentially including material parameter stochasticity.

To perform the proposed mapping, an explicit formulation of the transformation between the deterministic and desired stochastic shape is required on the relevant boundaries. While satisfying results were obtained when reshaping a circle into an ellipse with a random small axis length, some discrepancies were observed. These are thought to arise from the PCE operations. Indeed, in the algebra proposed by Debusschere et al.[28] and as further detailed by Ammouche and Jérusalem,[19] some operations (e.g., square root) in the stochastic space introduce nonrecoverable approximations. It is expected that transformations of increasing complexity would be required for more realistic industrial applications. As the required operations grow in difficulty, the approximations introduced by our stochastic algebra might be greater. It is possible to reduce these deviations by increasing the order of the PCE, at the expense of an exponential growth of the number of degrees of freedom. Note that Blatman and Sudret[38] proposed a truncation of the PCE, based on hyperbolic index sets, which could be used as a cost-effective alternative to the "full" PCE used here.

The current implementation still calls for additional key features to reach maturity. While the proposed mathematical formulation can readily incorporate random field variables, coding efforts are still required to include them in silico for more realistic simulations. Since our previous work, additional effort has been made to allow for the integration of visco-elastoplastic, hyperelastic and biological constitutive models, although the latter two are not being shown here (they are available in the code). The perturbation method used to simplify the calculation of the tangent modulus in a visco-elastoplastic framework, see Appendix A, also affects the speed-up provided by our framework.

5 | CONCLUSION

With the addition of this work, we proposed here successfully an intrusive method to simultaneously propagate mechanical and topological uncertainties. This method leverages the advantages of APFEM, where only parameter bounds are needed. A single, though arguably larger, simulation gives an accurate metamodel of the surface response over the whole parameter space. Doing so, this approach provides an analytical formulation of the mechanical changes (e.g., nodal displacement, elemental stress values) occurring in a mechanical system submitted to a set of loading and boundary conditions as a function of the metaparameters dictating topological changes in the system (e.g., inclusion geometry). This is achieved without the need to run multiple simulations. While future development could focus on extending this framework to take into account cases where input parameters are random fields, this extension of APFEM has the potential to be a powerful tool for design purposes, by allowing reliable parametric analyses of engineered structures under simultaneous geometrical and mechanical uncertainties within one unique simulation.

ACKNOWLEDGMENTS

The authors acknowledge funding by the EPSRC Prosperity Partnership Grant EP/S005072/1. The authors would also like to thank Dr. Van Dung Nguyen for the fruitful discussions.

DATA AVAILABILITY STATEMENT

APFEM and its extension to geometrical uncertainties are implemented in the code MuPhiSim, available on https://github.com/muphisim.

ENDNOTE

*Here and subsequently, Greek letter indices correspond to the stochastic space.

ORCID

Antoine Jérusalem https://orcid.org/0000-0001-5026-8038

REFERENCES

1. Li Y, Xiao Y, Yu L, Ji K, Li D. A review on the tooling technologies for composites manufacturing of aerospace structures: materials, structures and processes. *Compos A: Appl Sci Manuf*. 2022;154:106762.
2. Wucher B, Lani F, Pardoen T, Bailly C, Martiny P. Tooling geometry optimization for compensation of cure-induced distortions of a curved carbon/epoxy C-spar. *Compos A: Appl Sci Manuf*. 2014;56:27-35.
3. Hsiao K, Gangireddy S. Investigation on the spring-in phenomenon of carbon nanofiber-glass fiber/polyester composites manufactured with vacuum assisted resin transfer molding. *Compos A: Appl Sci Manuf*. 2008;39:834-842.
4. Teoh K, Hsiao K. Improved dimensional infidelity of curve-shaped VARTM composite laminates using a multi-stage curing technique—experiments and modeling. *Compos A: Appl Sci Manuf*. 2011;42:762-771.
5. Harris J, McShane G. Metallic stacked origami cellular materials: additive manufacturing, properties, and modelling. *Int J Solids Struct*. 2020;185-186:448-466.
6. Liu L, Kamm P, García-Moreno F, Banhart J, Pasini D. Elastic and failure response of imperfect three-dimensional metallic lattices: the role of geometric defects induced by selective laser melting. *J Mech Phys Solids*. 2017;107:160-184.
7. Zhang H, Guilleminot J, Gomez L. Stochastic modeling of geometrical uncertainties on complex domains, with application to additive manufacturing and brain interface geometries. *Comput Methods Appl Mech Eng*. 2021;385:114014.
8. Caflisch R. Monte Carlo and quasi-Monte Carlo methods. *Acta Numer*. 1998;7:1-49.
9. Wang X, Yao L, Zou Z. Effect of loading level and axial distribution on uncertainty performance of turbine blade with geometric variations. *Aerosp Sci Technol*. 2022;129:107851.
10. Weiner N. The homogeneous chaos. *Am J Math*. 1938;60:897-936.
11. Sakata S, Ashida F, Kojima T. Stochastic homogenization analysis on elastic properties of fiber reinforced composites using the equivalent inclusion method and perturbation method. *Int J Solids Struct*. 2008;45:6553-6565.
12. Pivovarov D, Steinmann P. Modified SFEM for computational homogenization of heterogeneous materials with microstructural geometric uncertainties. *Comput Mech*. 2016;57:123-147.
13. Canuto C, Kozubek T. A fictitious domain approach to the numerical solution of PDEs in stochastic domains. *Numer Math*. 2007;107:257-293.
14. Nouy A, Clément A, Schoefs F, Moës N. An extended stochastic finite element method for solving stochastic partial differential equations on random domains. *Comput Methods Appl Mech Eng*. 2008;197:4663-4682.
15. Acharjee S, Zabaras N. Uncertainty propagation in finite deformations—a spectral stochastic Lagrangian approach. *Comput Methods Appl Mech Eng*. 2006;195:2289-2312.
16. Ghanem R, Spanos P. *Stochastic Finite Elements: A Spectral Approach*. Springer-Verlag; 1991.
17. Mohan P, Nair P, Keane A. Stochastic projection schemes for deterministic linear elliptic partial differential equations on random domains. *Int J Numer Methods Eng*. 2011;85:874-895.
18. Zheng Z, Valdebenito M, Beer M, Nackenhorst U. A stochastic finite element scheme for solving partial differential equations defined on random domains. *Comput Methods Appl Mech Eng*. 2023;405:115860.
19. Ammouche Y, Jérusalem A. A modular nonlinear stochastic finite element formulation for uncertainty estimation. *Comput Methods Appl Mech Eng*. 2022;396:115044.
20. Ammouche Y, Jérusalem A. The a posteriori finite element method (APFEM), a framework for efficient parametric study and Bayesian inferences. *Comput Methods Appl Mech Eng*. 2023;412:115996.
21. Xiu D, Karniadakis G. The Wiener-Askey polynomial chaos for stochastic differential equations. *SIAM J Sci Comput*. 2002;24:619-644.
22. Cameron R, Martin W. Transformations of wiener integrals under translations. *Ann Math*. 1944;45:386-396.
23. Arola D, Williams C. Estimating the fatigue stress concentration factor of machined surfaces. *Int J Fatigue*. 2002;24:923-930.
24. Chen X, Fang S, Chen H. Stress concentration factor and fatigue analysis of a lateral nozzle with local wall thinning. *Eng Fail Anal*. 2019;105:289-304.
25. Inglis C. Stresses in plates due to the presence of cracks and sharp corners. *Trans Inst Nav Archit*. 1913;55:219-241.
26. Tong L, Xu G, Yang D, Mashiri F, Zhao X. Stress concentration factors in CHS-CFSHS T-joints: experiments, FE analysis and formulae. *Eng Struct*. 2017;151:406-421.
27. Wang B, Zhao W, Du Y, Zhang G, Yang Y. Prediction of fatigue stress concentration factor using extreme learning machine. *Comput Mater Sci*. 2016;125:136-145.
28. Debusschere B, Najm H, Pebay P. Numerical challenges in the use of polynomial chaos representations for stochastic processes. *SIAM J Sci Comput*. 2004;26:698-719.
29. Ahammed M. Probabilistic estimation of remaining life of a pipeline in the presence of active corrosion defects. *Int J Press Vessels Pip*. 1998;75:321-329.
30. Fatoba O, Akid R. On the behaviour of small fatigue cracks emanating from corrosion pits: part I—the influence of mechanical factors. *Theor Appl Fract Mech*. 2022;117:103154.
31. Shi P, Mahadevan S. Damage tolerance approach for probabilistic pitting corrosion fatigue life prediction. *Eng Fract Mech*. 2001;68:1493-1507.

32. Cerit M. Corrosion pit-induced stress concentration in spherical pressure vessel. *Thin-Walled Struct*. 2019;136:106-112.
33. Zuñiga Tello I, Domínguez Almaraz G, López Garza V, Guzmán Tapia M. Numerical investigation of the stress concentration on 7075-T651 aluminum alloy with one or two hemispherical pits under uniaxial or biaxial loading. *Adv Eng Softw*. 2019;131:23-35.
34. Li X, Zhang L, Dong Y, Wei Z, Que Z, Qu X. Orientation relationship of texture development in hot-rolled w during annealing. *Int J Refract Met Hard Mater*. 2021;97:105527.
35. Stefanou G, Savvas D, Gavallas P, Papaioannou I. The effect of random field parameter uncertainty on the response variability of composite structures. *Compos Part C Open Access*. 2022;9:100324.
36. Thapa M, Missoum S. Uncertainty quantification and global sensitivity analysis of composite wind turbine blades. *Reliab Eng Syst Saf*. 2022;222:108354.
37. Rosić B, Kučerová A, Sýkora J, Pajonk O, Litvinenko A, Matthies H. Parameter identification in a probabilistic setting. *Eng Struct*. 2013;50:179-196.
38. Blatman G, Sudret B. Adaptive sparse polynomial chaos expansion based on least angle regression. *J Comput Phys*. 2011;230:2345-2367.

How to cite this article: Ammouche Y, Jérusalem A. Extension of the *a posteriori* finite element method (APFEM) to geometrical alterations and application to stochastic homogenisation. *Int J Numer Methods Eng*. 2024;125(14):e7482. doi: 10.1002/nme.7482

APPENDIX A.

This appendix details the visco-elastoplastic constitutive model used in Section 3.3 and the implementation of the radial return.

A.1 Details of the constitutive model

In this kinematic framework, the total deformation gradient $\boldsymbol{F}$ is decomposed into an elastic and plastic part:

$$\boldsymbol{F} = \boldsymbol{F^e} \cdot \boldsymbol{F^p}, \tag{A1}$$

where $\boldsymbol{F^e}$ and $\boldsymbol{F^p}$ are, respectively, the elastic and plastic parts of the deformation gradient. The second Piola–Kirchhoff stress, $\boldsymbol{S}$, is a function of the $\boldsymbol{F^e}$. The plastic flow is modelled using the J_2-flow theory where the evolution of $\boldsymbol{F^p}$ follows:

$$\dot{\boldsymbol{F}}^p \cdot (\boldsymbol{F}^p)^{-1} = \sqrt{\frac{3}{2}}\dot{\varepsilon}^p \boldsymbol{R}, \tag{A2}$$

where $\boldsymbol{R}$ is computed as follows:

$$\boldsymbol{R} = \frac{3}{2\sigma}\boldsymbol{C}_e \cdot \boldsymbol{S}_{\text{dev}} \cdot \boldsymbol{C}_e, \tag{A3}$$

where $\boldsymbol{C}_e = (\boldsymbol{F}^e)^T \cdot \boldsymbol{F}^e$ is the elastic right Cauchy–Green tensor, $\boldsymbol{S}_{\text{dev}}$ is the deviatoric part of $\boldsymbol{S}$ expressed as:

$$\boldsymbol{S}_{\text{dev}} = \boldsymbol{S} - \frac{1}{3}(\boldsymbol{S} : \boldsymbol{C}_e^{-1}) \cdot \boldsymbol{C}_e^{-1}, \tag{A4}$$

and σ is the equivalent stress defined as:

$$\sigma = \sqrt{\frac{3}{2}(\boldsymbol{S}_{\text{dev}} \cdot \boldsymbol{C_e}) : (\boldsymbol{C_e} \cdot \boldsymbol{S}_{\text{dev}})}. \tag{A5}$$

Finally, the evolution of the plastic effective strain rate $\dot{\varepsilon}^p$ is given by:

$$\dot{\varepsilon}^p = \dot{\varepsilon}_0 \left(\frac{\sigma}{s}\right)^n. \tag{A6}$$

The values of parameters $\dot{\varepsilon}_0$, σ and s used in Section 3.3 are defined in Table 5. In the proposed stochastic framework, when solving for $\boldsymbol{F^p}$ that verifies Equation (A2) (a nonlinear system), a perturbation algorithm is used.

A.2 Radial return algorithm

At a given time step t_{n+1}, the increment of the deformation gradient $\Delta \boldsymbol{F} = \boldsymbol{F}^{n+1} - \boldsymbol{F}^{n}$ is decomposed into two increments of elastic and plastic deformation gradient $\Delta \boldsymbol{F}^{e}$ and $\Delta \boldsymbol{F}^{p}$. The following function L_2 norm of the residual $\mathfrak{R}(\Delta \boldsymbol{F}^{e})$ defined as:

$$\mathfrak{R}(\Delta \boldsymbol{F}^{e}) = \dot{\boldsymbol{F}}^{p,n+1}(\boldsymbol{F}^{p,n+1})^{-1} - \sqrt{\frac{3}{2}}\dot{\epsilon}^{p}\boldsymbol{R}, \tag{A7}$$

is then minimised at every step to solve for $\Delta \boldsymbol{F}^{e}$ (and thus $\Delta \boldsymbol{F}^{p}$). For the sake of clarity, the time index $n+1$ is dropped here and subsequently. Minimising the L_2 norm of $\mathfrak{R}$ (i.e., numerically below a given tolerance κ_{tol}) is done here by making use of a Newton–Raphson algorithm. We recall that $\Delta \boldsymbol{F}^{e}$ is decomposed as $\Delta \boldsymbol{F}^{e} = \sum_{\alpha=0}^{N-1} \Delta \boldsymbol{F}^{e}_{\alpha} \Psi_{\alpha}$, where $\Delta \boldsymbol{F}^{e}_{\alpha}$ is a tensor of size n_{dim}^2, n_{dim} being the physical dimension of the problem. To this end, the following tangent modulus $\boldsymbol{T}$ has to be computed:

$$T_{\alpha ij \beta kl} = \frac{\partial \mathfrak{R}(\Delta \boldsymbol{F}^{e})_{\alpha ij}}{\partial \Delta F^{e}_{\beta kl}}. \tag{A8}$$

In this work, the perturbation method is used, see Algorithm 1.

We finally recall that the computation of $\mathfrak{R}(\Delta \boldsymbol{F}^{e})$ requires the evaluation of the constitutive law to compute $\boldsymbol{S}_{\text{dev}}$. Note that, as $\mathfrak{R}(\Delta \boldsymbol{F}^{e})$ is computed $N^2 n_{\text{dim}}^4$ times, the return radial algorithm can become expensive when the stochastic dimension N grows.

Algorithm 1. Stochastic radial return algorithm

Solve the equilibrium equation to obtain the total deformation increment $\Delta \boldsymbol{F}$.
Initialisation Assume a purely elastic increment $\Delta \boldsymbol{F}^{e} = \Delta \boldsymbol{F}$.
Compute the initial value of $||\mathfrak{R}(\Delta \boldsymbol{F}^{e})||_2$.
Set iteration count $ite = 0$.
if $||\mathfrak{R}(\Delta \boldsymbol{F}^{e})||_2 < \kappa_{\text{tol}}$ **then**
    $\Delta \boldsymbol{F}^{e} = \Delta \boldsymbol{F}$. Proceed to the next material point.
else
    while $||\mathfrak{R}(\Delta \boldsymbol{F}^{e})||_2 > \kappa_{\text{tol}}$ and $ite < ite_{\max}$ **do**
        for $\alpha = 0$ to N-1 **do**
            for i=0 to $n_{\text{dim}} - 1$ **do**
                for j=0 to $n_{\text{dim}} - 1$ **do**
                    for $\beta = 0$ to N-1 **do**
                        for k=0 to $n_{\text{dim}} - 1$ **do**
                            for l=0 to $n_{\text{dim}} - 1$ **do**
                                Set $\Delta F^{e,\text{trial}}_{\beta kl} = \Delta F^{e}_{\beta kl} + \delta$.
                                Compute the perturbed value of $\mathfrak{R}(\Delta \boldsymbol{F}^{e})_{\text{perturbed}}$.
                                Compute and store the value of $T_{\alpha ij \beta kl} = \frac{\mathfrak{R}(\Delta \boldsymbol{F}^{e})_{\alpha ij,\text{perturbed}} - \mathfrak{R}(\Delta \boldsymbol{F}^{e})_{\alpha ij}}{\delta}$.
                            end for
                        end for
                    end for
                end for
            end for
        end for
        Update $\Delta \boldsymbol{F}^{e} = \Delta \boldsymbol{F}^{e} - \boldsymbol{T}^{-1} \cdot \mathfrak{R}(\Delta \boldsymbol{F}^{e})$.
        Update the value of $\mathfrak{R}(\Delta \boldsymbol{F}^{e})$.
        $ite = ite + 1$.
    end while
end if